Characterization of Angular Noise Coupling into Differential Arm Length of the LIGO Livingston Detector Interim #2

Brian C. Seymour,[1] Marie Kasprzack,[2] Arnaud Pelé,[2] and Adam Mullavey[2]

[1]*LIGO SURF Student, University of Virginia*[*]
[2]*LIGO SURF Mentor, LIGO Livingston Observatory*
(Dated: August 4, 2017)

Mirror misalignments of the Fabry Perot Cavity mirrors can change the cavity length. This source of noise can couple into differential arm length of a gravitational wave detector. This paper explores length change due to angular misalignment, and then extends it to the effect of angular noise on the two cavity system. We will also provide results from an experiment where we use mechanical modulation to measure the main angular components that are believed to couple most strongly to the differential arm length. The angular noise coupling model and experimental results will be used in combination to understand the angular noise contribution to differential arm length noise.

I. Introduction

In 1916 gravitational waves were predicted by Albert Einstein as a byproduct of his general theory of relativity which describes the relation between spacetime and matter. Just as accelerating charges emit light in classical electrodynamics, gravitational waves are emitted by accelerating masses. Gravitational waves travel at the speed of light in vacuum but, contrary to the latter, they are not obstructed by matter [1].

Gravitational waves will lead to new physics and astrophysics to examine the universe in complement to the existing information such as electromagnetic radiation and particles. Since gravity is much weaker than the other four fundamental forces, it is challenging to set up an experiment with gravity due to the large scale required to observe it. Thus, research in gravity is done by observing astrophysical signals around us, and gravitational waves will provide a new way to see more direct influences of the effects of gravity [2]. Additionally, predictions of general relativity can be compared to the gravitational wave data to test the validity limits of the theory. Lastly, gravitational wave astronomy will open a myriad of astronomical data, from examining black holes to probing past the cosmic microwave background. The cosmic microwave background may include a gravitational wave background, which would be evidence for inflation.

Laser Interferometer Gravitational-Wave Observatory (LIGO) is a collaboration dedicated to finding gravitational waves. It consists of two main facilities in Livingston, Louisiana and Hanford, Washington. These facilities detect gravitational waves with an optical system based on the interferometer developed by Michelson and Morley. Each observatory consists of a Michelson interferometer with 4 kilometer arms which measure the deformation of space produced by gravitational wave by looking for intensity variations in the interference pattern. It contains Fabry-Perot cavities which allows the light to bounce along the arms about 280 times. It uses light recycling to increase the power of a 25W laser into a 100KW laser in the arms. The laser also travels through a vacuum and dampens out environmental vibrations both actively and passively. The main optics are suspended with four stages of pendulums to passively isolate them from ground motion, and is kept at its operating point by active control through a plethora of feedback and feedforward techniques.

After LIGO searched for gravitational waves in the 2000's with no clear detections. Afterwards, the detectors were upgraded via the Advanced LIGO project. With these improvements, in September 2015, LIGO detected the first gravitational wave, and they had a second detection in December 2015 [3, 4]. Both of these detections were due to binary black hole system rotating and then combining.

In order to keep the mirrors stable, LIGO uses an active alignment sensing and control system (ASC) to reduce the mirror's angular motion [5]. Currently, the low frequency sensitivity (10-15 Hz) of the LIGO Livingston instrument is limited by the angular control feedback loops. To reduce the noise in this frequency band, the angular noise to DARM coupling should be reduced below 1/10th of the design sensitivity at that frequency [5].

II. Work Done

- Gained familiarity with techniques used by reading references provided. This includes gaining more knowledge in the following:

  - interferometric gravitational wave detector workings

  - Control systems

  - Digital signal processing and data analysis (specifically random data analysis)

  - Wiener filtering and spectral subtraction

  - Better knowledge of optics to better understand angular sensing and control
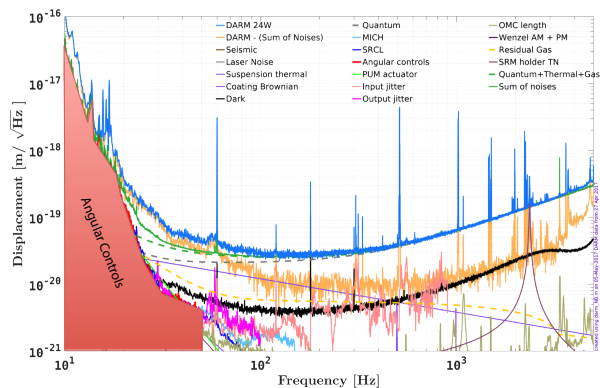
[*] Seymour.BrianC@gmail.com

FIG. 1. Notice the sharp uptick in angular noise 25Hz, where it quickly becomes the dominant source of noise at 10Hz [6].

- Learned about LIGO instrument and focus on angular control systems and incorporate knowledge gained from the readings with feedback and feedforward control systems.

- Learned about WFS, ADS, Optical Lever, and other ASC systems in LIGO.

- Practiced some discrete fast fourier transform and power spectrum problems with Matlab.

- Learned about the tools to take necessary online data. Measurements templates will be created with the online LIGO tool DTT or generated with Matlab depending on the progress.

- Worked on a model for change in cavity length in the Fabry-Perot Cavity with a Gaussian beam.

- Used the hard-soft basis to in the model to remove cross couplings in length change.

- Found length change for hard-soft in yaw.

- Generalized cavity length change model to the two cavity system of LIGO.

- Made model in the differential hard basis that LIGO uses.

- Did theoretical work for an experiment to produce spectra for angles.

- Performed mechanical modulation experiment.

- Did some calibration for the output of the experiment.

III. Change in Cavity Length in Fabry-Perot Cavity

III.1. Beam Spot Motion Approach to Angular Noise

In the interferometer cavity, angular rotations can create noise by coupling to cavity length. This is because the beam is not centered the mirror's center of rotation, and this distance is called static beam spot offset. When the mirror rotates slightly, this causes a change in cavity length (eq (1)). The equation depends on frequency however, and for the Fourier transform of equation (1), both the beam spot offset and mirror angle depend on frequency. The convolution can be approximated as in equation (2) [5].

$$\Delta l(t) = d_{spot}(t) \times \theta_{mirror}(t) \tag{1}$$

$$
\begin{aligned}
\Delta L(f) &= D_{spot}(f) * \Theta_{mirror}(f) \\
&\approx d_{spot}^{RMS} \times \Theta_{mirror}(f) + \theta_{mirror}^{RMS} \times D_{spot}(f)
\end{aligned} \tag{2}
$$

III.2. Cavity Misalignments

A laser beam in the Fabry-Perot cavity is shifted away due to angular misalignment in the cavity mirrors. The length of the cavity that the light beam travels is changed. This manuscript will describe methods to deduce both the beam position displacement and corresponding length changes as shown in Figure 2. The resulting change in cavity length from both arms contributes to the noise seen by the DARM channel.

A beam in the Fabry-Perot cavity must go through the two centers of curvature of the mirrors. So, when the mirrors rotate, their centers of curvature change. This causes the beam line to change. We have two x and two z coordinates from the centers of curvature here to define the line, and we will use these to find the points that the beam hits the mirrors.

III.3. Change in Cavity Length

If a beam hits the mirrors at points (z_1, x_1) and (z_2, x_2), the change in cavity length, ΔL, can be found. Note, the angles and center of curvature coordinates are implicitly in the variables of equation (3). The initial cavity length before perturbation is L.

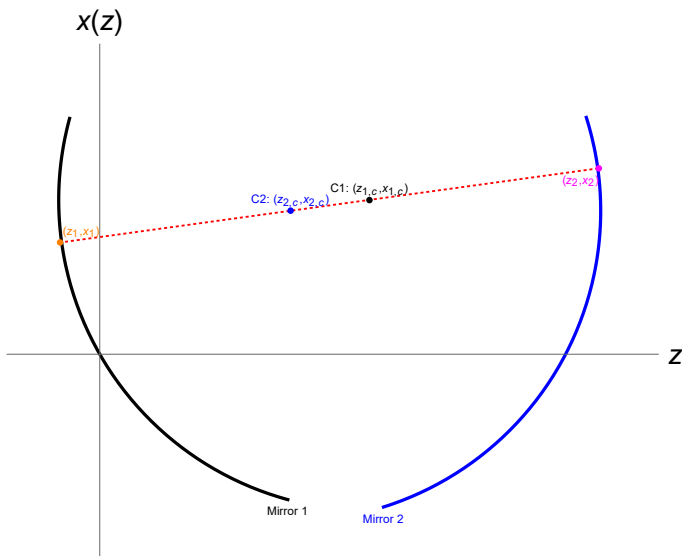$$\Delta L = L' - L = \sqrt{(x_2 - x_1)^2 + (z_2 - z_1)^2} - L \tag{3}$$

FIG. 2. This figure shows the setup of the mirrors. The points in the middle are the locations of the center of curvatures of each mirror. The points on the mirror are coordinates that this paper desires to find.

III.4. Beam Reflection Location in Fabry-Perot Cavity

The left mirror is the input test mass (ITM) in this paper and the right mirror is the end test mass (ETM). For notation simplicity, the ITM angle is θ_1 (CCW convention) and the ETM angle is θ_2 (CW convention) with both measuring the angular misalignment. Let x be the height of the beam at position z horizontally. The following constants are the locations of the center of curvature of mirror 1 and 2.

$$\begin{cases} z_{1c} = R_1 \cos(\theta_1) \\ x_{1c} = R_1 \sin(\theta_1) \\ z_{2c} = L - R_2 \cos(\theta_2) \\ x_{2c} = R_2 \sin(\theta_2) \end{cases} \quad (4)$$

The beam line pictured in red must go through the two centers of curvature. Therefore the slope, m, can be obtained.

$$\begin{aligned} m &= \frac{x_{1c} - x_{2c}}{z_{1c} - z_{2c}} \\ &= \frac{R_1 \sin(\theta_1) - R_2 \sin(\theta_2)}{R_1 \cos(\theta_1) + R_2 \cos(\theta_2) - L} \end{aligned} \quad (5)$$

The beam path is given in equation (6). The equations for the mirror curves are in equations (7) and (8).

$$\begin{cases} x_{beam}(z) = x_{1c} + m(z - z_{1c}) & (6) \\ R_1^2 = (x(z) - x_{1c})^2 + (z - z_{1c})^2 & (7) \\ R_2^2 = (x(z) - x_{2c})^2 + (z - z_{2c})^2 & (8) \end{cases}$$

What remains to be found is the points of intersection of the beam and the mirrors. Substituting $x_{beam}(z)$ into the mirror equations, the solution emerges in equation (12):

$$R_1^2 = (x_{1c} + m(z - z_{1c}) - x_{1c})^2 + (z - z_{1c})^2 \quad (9)$$

$$R_1^2 = (m(z - z_{1c}))^2 + (z - z_{1c})^2 \quad (10)$$

$$R_1^2 = (m^2 + 1)(z - z_{1c})^2 \quad (11)$$

$$z = z_{1c} \pm \frac{R_1}{\sqrt{m^2 + 1}} \quad (12)$$

By symmetry the second intersection can be found. The extraneous roots are removed since the angle is less than $\pi/2$ radians (eq (13a) and (13b)). The coordinates of the beam spot are $(z_1, x(z_1))$ and $(z_2, x(z_2))$. Thus ΔL can be determined from these coordinates when placed in (3).

$$z_1 = z_{1c} - \frac{R_1}{\sqrt{m^2 + 1}} \quad (13a)$$

$$z_2 = z_{2c} + \frac{R_2}{\sqrt{m^2 + 1}} \quad (13b)$$

III.5. Change in Cavity Length to the Second Order

A second order approximation for equation (3) can be found around the point $(\theta_1, \theta_2) = (0, 0)$ now that the values in equations (13a) and (13b) have been found. This is shown in equation (14). A discussion about how this was found is through Mathematica is located in appendix A. The g factors are unitless constants; in real system their values are: $g_1 = g_{itm} = -1.0655$ and $g_2 = g_{etm} = -.7794$ [7].

$$\Delta L \approx \Delta L_{2nd} = \frac{L}{2(1 - g_1 g_2)}(g_2 \theta_1^2 + 2\theta_1 \theta_2 + g_1 \theta_2^2) \quad (14)$$

$$g_i = 1 - \frac{L}{R_i}$$

IV. Hard and Soft Basis

IV.1. Motivation of Hard-Soft Basis from Radiation Pressure

When the beam is not aligned with the cavity axis, the radiation pressure of the beam exerts a torque on the mirrors. This reduces the pendulum restoring torque by the mirror suspension which can increase misalignment. Radiation pressure torque depends on the beam spot displacement. Equation (16) shows the value of the radiation pressure torque as a function of angle by linking it with equation (15) [8].

$$\vec{x}_{sa} = \begin{bmatrix} x_{1,sa} \\ x_{2,sa} \end{bmatrix} = \frac{L}{1 - g_1 g_2} \begin{bmatrix} g_2 & 1 \\ 1 & g_1 \end{bmatrix} \begin{bmatrix} \theta_1 \\ \theta_2 \end{bmatrix} \quad (15)$$
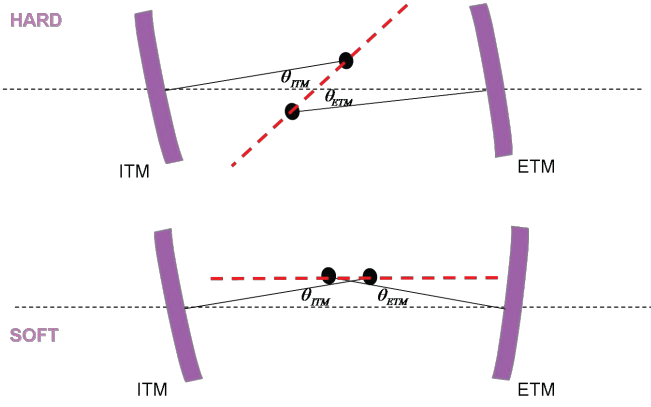
FIG. 3. This picture shows what the soft-hard basis angles look like in the cavity. This figure originated in [5].

FIG. 4. This figure shows how the cavity length changes as a function of the soft and hard modes.

$$\vec{\tau}_{opt} = \frac{2P}{c}\begin{bmatrix} x_1 \\ x_2 \end{bmatrix} = -\boldsymbol{K_{opt}}\begin{bmatrix} \theta_1 \\ \theta_2 \end{bmatrix} \qquad (16)$$

Equation (16) gives a differential equation for torque. The hard-soft basis is one that diagonalizes the $\boldsymbol{K_{opt}}$ matrix in order to solve the differential equation (17) [8]. Equation (18) is the change of basis matrix for the diagonalization [5].

$$\vec{\tau}_{ext} = \boldsymbol{I}\ddot{\vec{\theta}} + \boldsymbol{\gamma}\dot{\vec{\theta}} + (\boldsymbol{\kappa_p} + \boldsymbol{K_{opt}})\,\vec{\theta} \qquad (17)$$

$$\boldsymbol{S} = \begin{bmatrix} 1 & -r \\ r & 1 \end{bmatrix} \qquad (18)$$

$$r = \frac{(g_1 - g_2) + \sqrt{(g_1 - g_2)^2 + 4}}{2} \qquad (19)$$

As laser power increases in the cavity, eigenvectors of the $\boldsymbol{K_{opt}}$ have a negative restoring spring constant. As radiation pressure increases, the eigenvalue for the spring constant k_{soft} decreases in equation (20). Thus, control systems designed to mitigate this are used to keep the mirror alignment at its operating point.

$$\boldsymbol{S} \times \boldsymbol{K_{opt}} \times \boldsymbol{S^{-1}} = \begin{bmatrix} k_{soft} & 0 \\ 0 & k_{hard} \end{bmatrix} \qquad (20)$$

This radiation pressure example has motivated an interesting soft-hard basis with nice properties. The hard mode represents rotation of the cavity axis, and the soft mode represents a vertical displacement of the cavity axis. Figure 3 shows this.

IV.2. The Cavity Length Change Approximation in Hard-Soft Basis

Cavity length change equation (14) can be converted into the hard-soft basis. Just as it diagonalized the radiation pressure matrix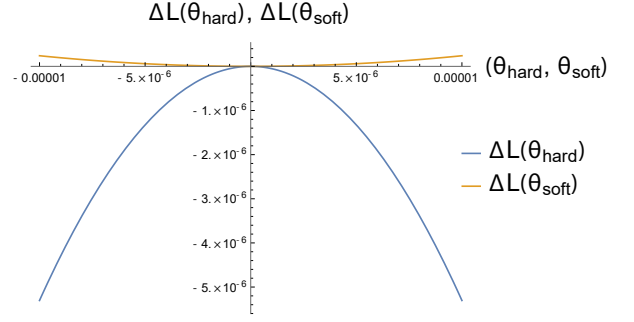, it removes the cross terms from the cavity length change equation. The result is below in equation (21). The second equation includes the numerical values for the LIGO Livingston interferometer, which is calculated by using g factors and the initial cavity length.

$$\Delta L = \frac{L}{2(1 - g_1 g_2)}\Big[\theta_{soft}^2(g_1 r^2 + 2r + g_2) \\ + \theta_{hard}^2(g_2 r^2 - 2r + g_1)\Big] \qquad (21)$$

$$\Delta L = 1810.49\,\theta_{soft}^2 - 39883.9\,\theta_{hard}^2 \qquad (22)$$

This equation for hard and soft modes is shown in figure 4.

V. Two Cavity Picture for Angle-to-Length Coupling

V.1. Two Cavity DARM Coupling

Since the principle concern for angle to length coupling is it's effect on DARM, equation (14) can be extended to find the effect of its coupling to DARM by subtracting the X arm length change from the Y arm length change. The resulting change in DARM due to angular noise is in equation (23).

$$\Delta D = \Delta L_x - \Delta L_y \\ = \frac{L}{2 - 2g_1 g_2}\Big((\theta_{ex}^2 g_1 + 2\theta_{ex}\theta_{ix} + g_2\theta_{ix}^2) \\ - (\theta_{ey}^2 g_1 + 2\theta_{ey}\theta_{iy} + g_2\theta_{iy}^2)\Big) \qquad (23)$$

V.2. Pitch and Yaw Convention

Until this point, the paper has worked the pitch case. The coordinate systems of the test masses are local, with the normal vector $\hat{z}$ pointing towards the other test mass

and $\hat{x}$ pointing up. Since $\hat{y} = \hat{z} \times \hat{x}$, the transverse unit vectors point in the opposite direction, $\hat{y}_2 = -\hat{y}_1$. Thus, the yaw change of basis matrix acquires an extra minus sign in the second column of equation (24b) [9]. The relationship between bases is in equation (24c).

$$\boldsymbol{S}_{pitch} = \begin{bmatrix} 1 & -r \\ r & 1 \end{bmatrix} \tag{24a}$$

$$\boldsymbol{S}_{yaw} = \begin{bmatrix} 1 & -r \\ -r & -1 \end{bmatrix} \tag{24b}$$

$$\vec{\theta} = \begin{bmatrix} \theta_1 \\ \theta_2 \end{bmatrix} = \boldsymbol{S} \times \begin{bmatrix} \theta_{soft} \\ \theta_{hard} \end{bmatrix} = \boldsymbol{S} \times \vec{\theta}' \tag{24c}$$

V.3. Differential/Common Hard/Soft Basis

In the two cavity case, it is useful to separate the hard/soft basis in cavity X and Y into the differential/common modes. For example, differential hard is X hard minus Y hard. The change of basis matrix is in equation (25). [5]:

$$\begin{pmatrix} \theta_{dif,h} \\ \theta_{dif,s} \\ \theta_{com,h} \\ \theta_{com,s} \end{pmatrix} = \frac{1}{2} \begin{pmatrix} 0 & 0 & 1 & -1 \\ 1 & -1 & 0 & 0 \\ 0 & 0 & 1 & 1 \\ 1 & 1 & 0 & 0 \end{pmatrix} \begin{pmatrix} \theta_{s,x} \\ \theta_{s,y} \\ \theta_{h,x} \\ \theta_{h,y} \end{pmatrix} \tag{25}$$

Equation (26) shows how the differential hard basis is related back to the mirror basis for both pitch and yaw [5]

$$\begin{pmatrix} \theta_{ix} \\ \theta_{iy} \\ \theta_{ex} \\ \theta_{ey} \end{pmatrix}_p = \begin{pmatrix} -r & 1 & -r & 1 \\ r & -1 & -r & 1 \\ 1 & r & 1 & r \\ -1 & -r & 1 & r \end{pmatrix} \begin{pmatrix} \theta_{dh} \\ \theta_{ds} \\ \theta_{ch} \\ \theta_{cs} \end{pmatrix}_p \tag{26a}$$
$$\vec{\theta}_p = \boldsymbol{Q}_p \cdot \vec{\theta}_p'$$

$$\begin{pmatrix} \theta_{ix} \\ \theta_{iy} \\ \theta_{ex} \\ \theta_{ey} \end{pmatrix}_y = \begin{pmatrix} r & 1 & r & 1 \\ r & 1 & -r & -1 \\ 1 & -r & 1 & -r \\ 1 & -r & -1 & r \end{pmatrix} \begin{pmatrix} \theta_{dh} \\ \theta_{ds} \\ \theta_{ch} \\ \theta_{cs} \end{pmatrix}_y \tag{26b}$$
$$\vec{\theta}_y = \boldsymbol{Q}_y \cdot \vec{\theta}_y'$$

Equation (23) for angular noise DARM coupling becomes equation (27) in the differential hard basis angular coupling to DARM. In β, pitch is + and yaw is -. Interestingly, the all the terms are multiples of common times differential modes.

Appendix E discusses CARM with the opposite case, where terms are multiples of only common times common and differential times differential modes.

$$\Delta D = \alpha \theta_{ch}\theta_{dh} + \beta\theta_{ch}\theta_{ds} + \beta\theta_{cs}\theta_{dh} + \gamma\theta_{cs}\theta_{ds} \tag{27a}$$

$$\mu = \frac{2L}{-1 + g_1 g_2} \tag{27b}$$

$$\alpha = \mu(-g_1 r^2 - g_2 + 2r) = -156191 \tag{27c}$$

$$\beta = \pm\mu(-g_1 r + g_2 r - r^2 + 1) = \pm 23379.1 \tag{27d}$$

$$\gamma = \mu(-r(g_2 r + 2) - g_1) = 3897.58 \tag{27e}$$

V.4. Spectra of Angle to DARM Coupling

Consider the following situation where the DARM coupling is expressed as follows:

$$\Delta D(t) = \alpha\,\theta_{dh}(t)\theta_{ch}(t) \tag{28}$$

In the frequency domain:

$$\Delta D(f) = \alpha\,\hat{\theta}_{dh}(f) \star \hat{\theta}_{ch}(f) \tag{29}$$

Unfortunately, we are in the same situation as equation (2) where the convolution presents a problem. Thus to understand the effect on DARM of angular misalignment, the spectra of angles in the hard-soft basis must be found.

VI. Finding Spectra through Mechanical Modulation

In order to measure the spectra of the angles of the hard-soft basis, mechanical modulation will be used. Currently, the ADS system is used to align the cavity by modulation/demodulation at frequencies of 7 Hz, below the detection band. The demodulated output effectively measures the degree of freedom. This sensing method is similar to the optical modulation methods in the WFS and allows the actuators to correct for errors [10]. Appendix C gives an example of how mechanical modulation is used in LIGO to detect misalignments.

We will use this sensing method by dithering at a higher frequency to measure the spectra of the differential hard and common hard angular degrees of freedom. The dithering frequency used in the experiment was 48.7 Hz. Our witness is DARM channel which is demodulated and applied with a lowpass filter.

VI.1. Mirror Angle Modulation Coupling to DARM

Equation (27) links the mirror degrees of freedom to change in DARM. Each degree of freedom is dithered according to the dithering parameters in 30a. $\Theta(t)$ is the residual motion of the mirror which causes misalignment and the $\sin\Omega t$ term is the dithering term from our hardware injection. The DARM channel is multiplied by 30b

in order to demodulate it.

$$\theta_{dh}(t) = \Theta_{dh}(t) + A_{dh}\sin\Omega t$$
$$\theta_{ds}(t) = \Theta_{ds}(t) + A_{ds}\sin\Omega t$$
$$\theta_{ch}(t) = \Theta_{ch}(t) + A_{ch}\sin\Omega t \tag{30a}$$
$$\theta_{cs}(t) = \Theta_{cs}(t) + A_{cs}\sin\Omega t$$

$$O_{dmod} = A_{\text{dmod}}\sin\Omega t \tag{30b}$$

After modulating and demodulating equation (27) a lowpass filter is applied. The lowpass filter should reject all contributions from an Ω term and above. The result of this lowpass filter is equation (31). The each angle's coefficient for this equation is shown below in 31b. Note how this resulting spectra is a linear combination of all the degrees of freedom. We would like to find, however, the spectra of each mode.

$$\text{LP}(\Delta\text{D}\cdot O_{\text{dmod}}) = C_{dh}\Theta_{dh} + C_{ds}\Theta_{ds}$$
$$+ C_{ch}\Theta_{ch} + C_{cs}\Theta_{cs} \tag{31a}$$

$$\begin{cases} C_{dh} = \dfrac{A_{\text{dmod}}}{2}\left(\alpha A_{\text{ch}} + \beta A_{\text{cs}}\right) \\[2ex] C_{ds} = \dfrac{A_{\text{dmod}}}{2}\left(\beta A_{\text{ch}} + \gamma A_{\text{cs}}\right) \\[2ex] C_{ch} = \dfrac{A_{\text{dmod}}}{2}\left(\alpha A_{\text{dh}} + \beta A_{\text{ds}}\right) \\[2ex] C_{cs} = \dfrac{A_{\text{dmod}}}{2}\left(\beta A_{\text{dh}} + \gamma A_{\text{ds}}\right) \end{cases} \tag{31b}$$

VI.2. Finding Spectra of Individual Modes

Since the constants in 31b are functions of the dithering amplitudes of each mode, the amplitudes can be chosen to zero out all but one of the coefficients. This desired modulation acquires the desired output which is only dependent on one mode. This section will discuss how to pick the correct amplitudes. First, a linear system is set up.

$$\begin{pmatrix} C_{\text{dh}} \\ C_{\text{ds}} \\ C_{\text{ch}} \\ C_{\text{cs}} \end{pmatrix} = \frac{A_{\text{dmod}}}{2}\begin{pmatrix} 0 & 0 & \alpha & \beta \\ 0 & 0 & \beta & \gamma \\ \alpha & \beta & 0 & 0 \\ \beta & \gamma & 0 & 0 \end{pmatrix}\cdot\begin{pmatrix} A_{\text{dh}} \\ A_{\text{ds}} \\ A_{\text{ch}} \\ A_{\text{cs}} \end{pmatrix} \tag{32}$$

Since we desire to find the amplitudes in terms of the coefficients, the system is inverted. This system shows how to choose dithering amplitudes for a desired demodulated result. For example, by setting C_{dh} to 1 and the other constants to zero, the resulting spectrum is proportional to Θ_{dh} in the demodulated output. This amplitude selection is a convenient way to measure spectra. (from now on, A_{dmod} will be set equal to 1)

$$\begin{pmatrix} A_{\text{dh}} \\ A_{\text{ds}} \\ A_{\text{ch}} \\ A_{\text{cs}} \end{pmatrix} = \frac{2}{\alpha\gamma - \beta^2}\begin{pmatrix} 0 & 0 & \gamma & -\beta \\ 0 & 0 & -\beta & \alpha \\ \gamma & -\beta & 0 & 0 \\ -\beta & \alpha & 0 & 0 \end{pmatrix}\begin{pmatrix} C_{\text{dh}} \\ C_{\text{ds}} \\ C_{\text{ch}} \\ C_{\text{cs}} \end{pmatrix} \tag{33}$$

Since the mirrors are driven according to their own local angles, the change of basis matrix $\boldsymbol{Q}$ from equation (27) is used. Equations (34) and (35) give these modulation amplitudes in the local mirror angle basis. The full form of these matrices is given in appendix B.

$$\begin{pmatrix} A_{ix} \\ A_{iy} \\ A_{ex} \\ A_{ey} \end{pmatrix}_p = \frac{2}{\alpha\gamma - \beta^2}\,\boldsymbol{Q}_p\cdot\begin{pmatrix} 0 & 0 & \gamma & -\beta \\ 0 & 0 & -\beta & \alpha \\ \gamma & -\beta & 0 & 0 \\ -\beta & \alpha & 0 & 0 \end{pmatrix}\begin{pmatrix} C_{\text{dh}} \\ C_{\text{ds}} \\ C_{\text{ch}} \\ C_{\text{cs}} \end{pmatrix}_p \tag{34}$$

$$\begin{pmatrix} A_{ix} \\ A_{iy} \\ A_{ex} \\ A_{ey} \end{pmatrix}_y = \frac{2}{\alpha\gamma - \beta^2}\,\boldsymbol{Q}_y\cdot\begin{pmatrix} 0 & 0 & \gamma & -\beta \\ 0 & 0 & -\beta & \alpha \\ \gamma & -\beta & 0 & 0 \\ -\beta & \alpha & 0 & 0 \end{pmatrix}\begin{pmatrix} C_{\text{dh}} \\ C_{\text{ds}} \\ C_{\text{ch}} \\ C_{\text{cs}} \end{pmatrix}_y \tag{35}$$

VI.3. Mirror Angle Calibration

In order to change the angle of a test mass, the penultimate test mass (PUM) actuators apply a torque. The torque arm distance is $\frac{d}{\sqrt{2}}$ and there are torques applied in the OSEM system, where d = 100mm. Equation (36) gives the amount of angle change due to the counts. It is from equation 44 of [9]. TF(f) is the transfer function between torque on the penultimate test mass to angle of the end test mass. It was calculated by a model detailed in that paper [9]. At f = 48.7Hz, the result is:

$$C_\theta = 2\sqrt{2}*d*F_0*\text{TF}_\theta(f)$$
$$C_\theta = 1.694\times10^{-18}\frac{\text{rad}}{\text{cts}} \tag{36a}$$

$$C_\phi = 2\sqrt{2}*d*F_0*\text{TF}_\phi(f)$$
$$C_\phi = 2.074\times10^{-18}\frac{\text{rad}}{\text{cts}} \tag{36b}$$

F_0 is created by a digital signal which is converted into volts, which is converted into current, which is used to create a magnetic field. This magnetic field exerts a force on the PUM. The numerical values are shown in equation (37), which are found in [11].

$$F_0 = \frac{20}{2^{18}}\frac{\text{V}}{\text{cts}}\cdot0.268\frac{\text{mA}}{\text{V}}\cdot0.0309\frac{\text{N}}{\text{A}}$$
$$= 6.318\times10^{-10}\frac{\text{N}}{\text{cts}} \tag{37}$$

Thus, equation (38) shows the formula for the calibrated C_{dh} in pitch, where (a_{ch}, a_{cs}) are the uncalibrated modulation amplitudes.

$$C_{dh} = A_{dmod}\cdot\frac{C_\theta}{2}(\alpha a_{ch} + \beta a_{cs}) \tag{38}$$

Appendix D gives a calibration flowchart summarizing this calibration process.

VI.4. Amplitude Spectrum Measurement for a Mode

In order to get the spectra of the differential hard mode, the amplitudes are set accordingly. The resulting equation of the measurement is in equation (39). $\mathcal{A}(f)$ is the measurement of the demodulated DARM channel's amplitude spectral density in counts, and $C_{\mathcal{A}}$ is the calibration.

$$\Theta_{dh}(f) = \frac{C_{\mathcal{A}}}{C_{dh}} \cdot \mathcal{A}(f) \tag{39}$$

$$\frac{1}{C_{\mathcal{A}}} = 6 \times 10^{17} \frac{\text{cts}}{m}$$

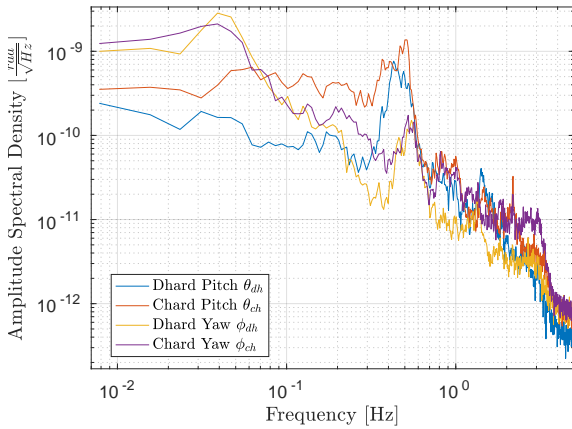The result of this technique is in figure 5 which shows the spectrum of the calibrated signal.

FIG. 5. This figure shows the result for the measured spectra. Above 3 Hz the signal is mostly noise.

VII. Future Inquiry

Now that I have the data from the dithering experiment, I will work on doing more data analysis. Once I have my calibrated spectra, I will look at how to apply it to my model for cavity length change. The spectra may have patterns which allow for a good approximation for noise similar to equation (2). I plan on seeing if there is a suitable approximation for the angle to DARM coupling of equation (27).

[1] R. Kinney, A. Weinstein, O. Miyakawa, and R. Ward, LIGO Document Control Center , T050149 (2005).

[2] P. Saulson, *Fundamentals of Interferometric Gravitational Wave Detectors* (World Scientific, 1994) p. 299.

[3] B. P. Abbott and E. Al, Physical Review Letters **116**, 61102 (2016).

[4] B. P. Abbott and E. Al, Physical Review Letters **116**, 241103 (2016).

[5] L. Barsotti and M. Evans, LIGO Document Control Center , T0900511_v4 (2009).

[6] G. Vajente, LIGO Document Control Center , G1701262 (2017).

[7] K. L. Dooley, L. Barsotti, R. X. Adhikari, M. Evans, T. T. Fricke, P. Fritschel, V. Frolov, K. Kawabe, and N. Smith-Lefebvre, J. Opt. Soc. Am. A **30**, 2618 (2013).

[8] K. Dooley, *Design and Performance of High Laser Power Interferometers for Gravitational-wave Detection* (University of Florida, 2011).

[9] M. Kasprzack and H. Yu, LIGO Document Control Center , T1600397 (2016).

[10] K. Kawabe, N. Mio, and K. Tsubono, Applied optics **33**, 5498 (1994).

[11] J. Kissel, LIGO Document Control Center , T1100378 (2016).

A. Exact Results from Mathematica

This appendix has the exact values of the coordinates found in section III.4. It also has the full equation for ΔL that was found. Equation (A1) was used in Mathematica to find the Taylor series in equation (14) from section III.5.

$$\Delta L = \text{Abs}\left(L\sqrt{\frac{(R_1 \sin(\theta_1) - R_2 \sin(\theta_2))^2}{(-L + R_1 \cos(\theta_1) + R_2 \cos(\theta_2))^2} + 1} - R_1 \cos(\theta_1)\sqrt{\frac{(R_1 \sin(\theta_1) - R_2 \sin(\theta_2))^2}{(-L + R_1 \cos(\theta_1) + R_2 \cos(\theta_2))^2} + 1} \right.$$
$$\left. - R_2 \cos(\theta_2)\sqrt{\frac{(R_1 \sin(\theta_1) - R_2 \sin(\theta_2))^2}{(-L + R_1 \cos(\theta_1) + R_2 \cos(\theta_2))^2} + 1} + R_1 + R_2 \right) - L \tag{A1}$$

$$z_1 = R_1\left(\cos(\theta_1) - \frac{1}{\sqrt{\frac{(R_1 \sin(\theta_1) - R_2 \sin(\theta_2))^2}{(-L + R_1 \cos(\theta_1) + R_2 \cos(\theta_2))^2} + 1}} \right) \tag{A2}$$

$$x_1 = R_1\left(\sin(\theta_1) + \frac{R_1 \sin(\theta_1) - R_2 \sin(\theta_2)}{(L - R_1 \cos(\theta_1) - R_2 \cos(\theta_2))\sqrt{\frac{(R_1 \sin(\theta_1) - R_2 \sin(\theta_2))^2}{(-L + R_1 \cos(\theta_1) + R_2 \cos(\theta_2))^2} + 1}} \right) \tag{A3}$$

$$z_2 = \frac{R_2}{\sqrt{\frac{(R_1 \sin(\theta_1) - R_2 \sin(\theta_2))^2}{(-L + R_1 \cos(\theta_1) + R_2 \cos(\theta_2))^2} + 1}} + L - R_2 \cos(\theta_2) \tag{A4}$$

$$x_2 = R_1 \sin(\theta_1) + \frac{((R_1 \sin(\theta_1) - R_2 \sin(\theta_2)))}{-L + R_1 \cos(\theta_1) + R_2 \cos(\theta_2)}$$
$$\times \left(\frac{R_2}{\sqrt{\frac{(R_1 \sin(\theta_1) - R_2 \sin(\theta_2))^2}{(-L + R_1 \cos(\theta_1) + R_2 \cos(\theta_2))^2} + 1}} + L - R_1 \cos(\theta_1) - R_2 \cos(\theta_2) \right) \tag{A5}$$

B. Full Form of Dithering Matrices

$$\begin{pmatrix} A_{ix} \\ A_{iy} \\ A_{ex} \\ A_{ey} \end{pmatrix}_p = \frac{2}{\alpha\gamma - \beta^2} \begin{pmatrix} -\beta - \gamma r & \alpha + \beta r & -\beta - \gamma r & \alpha + \beta r \\ -\beta - \gamma r & \alpha + \beta r & \beta + \gamma r & -\alpha - \beta r \\ \gamma - \beta r & \alpha r - \beta & \gamma - \beta r & \alpha r - \beta \\ \gamma - \beta r & \alpha r - \beta & \beta r - \gamma & \beta - \alpha r \end{pmatrix} \begin{pmatrix} C_{dh} \\ C_{ds} \\ C_{ch} \\ C_{cs} \end{pmatrix}_p \tag{B1}$$

$$\begin{pmatrix} A_{ix} \\ A_{iy} \\ A_{ex} \\ A_{ey} \end{pmatrix}_y = \frac{2}{\alpha\gamma - \beta^2} \begin{pmatrix} \gamma r - \beta & \alpha - \beta r & \gamma r - \beta & \alpha - \beta r \\ \beta - \gamma r & \beta r - \alpha & \gamma r - \beta & \alpha - \beta r \\ \gamma + \beta r & r\alpha r - \beta & \gamma + \beta r & -\alpha r - \beta \\ -\beta r - \gamma & \beta + \alpha r & \gamma + \beta r & -\alpha r - \beta \end{pmatrix} \begin{pmatrix} C_{dh} \\ C_{ds} \\ C_{ch} \\ C_{cs} \end{pmatrix}_y \tag{B2}$$

$$\begin{pmatrix} A_{ix} \\ A_{iy} \\ A_{ex} \\ A_{ey} \end{pmatrix}_p = 10^{-4} \begin{pmatrix} -0.346205 & 3.05472 & -0.346205 & 3.05472 \\ -0.346205 & 3.05472 & 0.346205 & -3.05472 \\ -0.418406 & 1.93982 & -0.418406 & 1.93982 \\ -0.418406 & 1.93982 & 0.418406 & -1.93982 \end{pmatrix} \begin{pmatrix} C_{dh} \\ C_{ds} \\ C_{ch} \\ C_{cs} \end{pmatrix}_p \tag{B3}$$

$$\begin{pmatrix} A_{ix} \\ A_{iy} \\ A_{ex} \\ A_{ey} \end{pmatrix}_y = 10^{-4} \begin{pmatrix} 0.346205 & 3.05472 & 0.346205 & 3.05472 \\ -0.346205 & -3.05472 & 0.346205 & 3.05472 \\ -0.418406 & -1.93982 & -0.418406 & -1.93982 \\ 0.418406 & 1.93982 & -0.418406 & -1.93982 \end{pmatrix} \begin{pmatrix} C_{dh} \\ C_{ds} \\ C_{ch} \\ C_{cs} \end{pmatrix}_y \tag{B4}$$

C. Dithering Theory

This section is an example from Kawabe's discussion on how mechanical modulation is used to sense and actively suppress low frequency motion of test mass angles [10]. It aligns the beam axis with the cavity axis.

To simplify, both mirrors have the same radius of curvature. Let I be the intensity of reflected field. The following parameters are used: $a(\nu)$ and $a(\nu - \nu_{10})$ is cavity reflectance of the fundamental mode and the first higher mode respectively (which are both constant), a_x is the beam waist height and α_x is the angle of misalignment of the incident beam and the cavity axis, and w_0 is the width of the waist.

$$I = I_0 \left[|a(\nu)|^2 + \gamma \left(|a(\nu - \nu_{10})|^2 - |a(\nu)|^2 \right) \right] \tag{C1a}$$

$$\gamma := \left(\frac{a_x}{w_0} \right)^2 + \left(\frac{k w_0 \alpha_x}{2} \right)^2 \tag{C1b}$$

$$a_x = \frac{1}{2}(x_1 + x_2) \tag{C1c}$$

$$\alpha_x = \frac{1}{2R - L}(x_2 - x_1) \tag{C1d}$$

The modulations are:

$$x_1 = x_{10} + A_1 \sin \omega_1 t \tag{C2a}$$

$$x_2 = x_{20} + A_2 \sin \omega_2 t \tag{C2b}$$

Substituting these two modulations in the values for the beam waist displacement a_x and angle difference α_x into equation (C1a), and taking a taylor series to first order, the following result is found[10].

$$I \approx I_0 \left[\left\{ |a(\nu)|^2 + \gamma \left(|a(\nu - \nu_{10})|^2 - |a(\nu)|^2 \right) \right\} * \left\{ \gamma(x_{10}, x_{20}) + A_1 \sin \omega_1 t \left. \frac{\partial \gamma}{\partial x_1} \right|_{x_{10}} + A_2 \sin \omega_2 t \left. \frac{\partial \gamma}{\partial x_2} \right|_{x_{20}} \right\} \right] \tag{C3}$$

Applying narrow bandpass filters around each modulation frequency and demodulating, the DC terms remaining are the two partial derivatives. When the partial derivatives are expanded, they take the following form.

$$\left. \frac{\partial \gamma}{\partial x_1} \right|_{x_{10}} = \frac{1}{2w_0^2} \left(x_{10} + x_{20} + \left(\frac{L}{k w_0^2} \right)^2 (x_{10} - x_{20}) \right) \tag{C4a}$$

$$\left. \frac{\partial \gamma}{\partial x_2} \right|_{x_{20}} = \frac{1}{2w_0^2} \left(x_{10} + x_{20} - \left(\frac{L}{k w_0^2} \right)^2 (x_{10} - x_{20}) \right) \tag{C4b}$$

The demodulation sensor returns the values of the partial derivatives of γ with respect to x_1 and x_2, which is an error signal for the cavity. This is a linear system which can be solved for the center displacements. The misalignment signal it is sent to the actuators to align the cavity.

D.   Flowchart of Calibration
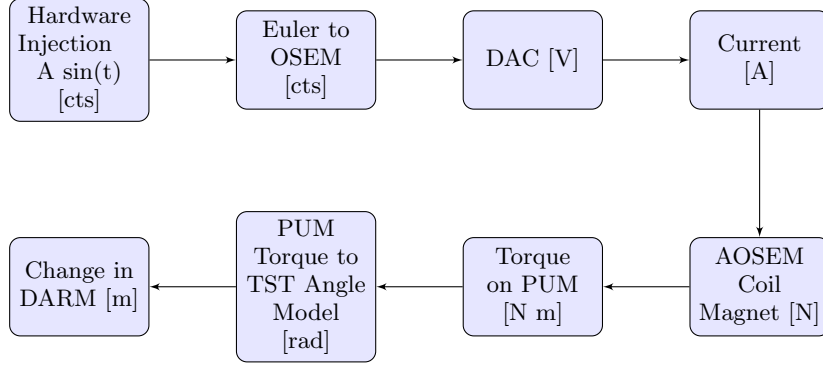
E.   Interesting findings from CARM/Interpretation of formula for DARM

When the formula for CARM is calculated, the following pattern emerges: all angles are either common squared or differential squared. This relates to DARM because retrospectively it can be seen that it is the product of a common and differential angle. Thus, solely common-differential mode products couple into DARM.

$$\Delta CARM = \frac{2\theta_{ch}\theta_{cs}L\left(g_1 r - g_2 r + r^2 - 1\right)}{g_1 g_2 - 1} + \frac{2\theta_{dh}\theta_{ds}L\left(g_1 r - g_2 r + r^2 - 1\right)}{g_1 g_2 - 1} - \frac{\theta_{ch}^2 L\left(r\left(g_1 r - 2\right) + g_2\right)}{g_1 g_2 - 1}$$
$$- \frac{\theta_{cs}^2 L\left(r\left(g_2 r + 2\right) + g_1\right)}{g_1 g_2 - 1} - \frac{\theta_{dh}^2 L\left(r\left(g_1 r - 2\right) + g_2\right)}{g_1 g_2 - 1} - \frac{\theta_{ds}^2 L\left(r\left(g_2 r + 2\right) + g_1\right)}{g_1 g_2 - 1} \tag{E1a}$$

$$\Delta CARM = -78095.7\theta_{ch}^2 + 23379.1\theta_{ch}\theta_{cs} + 1948.79\theta_{cs}^2 - 78095.7\theta_{dh}^2 + 23379.1\theta_{dh}\theta_{ds} + 1948.79\theta_{ds}^2 \tag{E1b}$$